Journal of Power and Energy Engineering, 2025, 13(9), 261-273
https://www.scirp.org/journal/jpee
ISSN Online: 2327-5901
ISSN Print: 2327-588X

Enhanced Incremental Conductance MPPT with Adjustable Reference Current and Scheduled-Gain Using a Power Zoning Strategy for Flyback-Based Photovoltaic Inverter Systems

Muhamad Faizal Yaakub[1,2*], Mohd Amran Mohd Radzi[2], Faridah Hanim Mohd Noh[3], Maaspaliza Azri[1], Suhaidi Shafie[2], Norhafiz Azis[2], AAhmad Naji Zaidan[4]

[1]Fakulti Teknologi dan Kejururteraan Elektrik, Universiti Teknikal Malaysia Melaka, Melaka, Malaysia
[2]Department of Electrical and Electronic Engineering, Universiti Putra Malaysia, Selangor, Malaysia
[3]Faculty of Engineering Technology, Universiti Tun Hussein Onn Malaysia, Batu Pahat, Malaysia
[4]College of Engineering, Al-Iraqia University, Baghdad Governorate, Iraq
Email: *muhamadfaizal@utem.edu.my

How to cite this paper: Yaakub, M.F., Radzi, M.A.M., Noh, F.H.M., Azri, M., Shafie, S., Azis, N. and Zaidan, A.N. (2025) Enhanced Incremental Conductance MPPT with Adjustable Reference Current and Scheduled-Gain Using a Power Zoning Strategy for Flyback-Based Photovoltaic Inverter Systems. *Journal of Power and Energy Engineering*, **13**, 261-273.
https://doi.org/10.4236/jpee.2025.139018

Received: September 1, 2025
Accepted: September 21, 2025
Published: September 24, 2025

Abstract

Efficient and reliable Maximum Power Point Tracking (MPPT) is crucial for photovoltaic (PV) systems, particularly under rapidly changing irradiance and temperature. This paper proposes an enhanced MPPT algorithm that extends the traditional Incremental Conductance (IncCond) method by introducing an adjustable reference current and scheduled-gain, coordinated through a power zoning strategy that suits current-source inverter or converter. Unlike conventional approaches based on voltage-source converters that adjust duty cycle or input voltage, the proposed method employs current-driven control tailored to distinct power regions, enabling faster and more accurate tracking. The algorithm was developed and validated in MATLAB/Simulink, providing a rigorous simulation environment to evaluate its dynamic performance. Results show that the proposed method achieves negligible overshoot, with deviations corrected in less than 16 milliseconds and maximum overshoot limited to under 2 W, even under extreme operating conditions such as 0˚C. Within normal operating ranges and near rated power, oscillations are minimal, overcoming the common drawbacks of conventional IncCond methods that suffer from slower convergence and steady-state oscillations. The findings confirm that the scheduled-gain power-zoning framework ensures a superior balance of transient speed, steady-state accuracy, and system stability, offering a practical and efficient solution for real-time PV applications in variable en-

vironments.

Keywords

Incremental Conductance, Maximum Power Point Tracking (MPPT), PV Inverter, Power Zoning, Schedule-Gain

1. Introduction

Photovoltaic (PV) systems are increasingly deployed across diverse scales. However, their intrinsic nonlinear current-voltage (I-V) and power-voltage (P-V) characteristics, together with rapid fluctuations in environmental conditions, often cause deviations from the maximum power point (MPP) unless advanced tracking algorithms are employed. Among the established maximum power point tracking (MPPT) techniques, the incremental conductance (IncCond) method is widely regarded as a reliable and robust solution, owing to its explicit application of the condition $dP/dV \approx 0$ at the MPP. Compared with the conventional perturb-and-observe (P&O) strategy, the IncCond algorithm generally exhibits superior dynamic responsiveness under irradiance transients. Recent investigations have further demonstrated its effectiveness in grid-connected architecture operating under rapidly changing conditions. Nonetheless, issues such as residual steady-state oscillations and reduced convergence speed during abrupt irradiance ramps persist [1] [2].

However, conventional IncCond faces well-known trade-offs between tracking speed and ripple due to fixed or coarsely scheduled step sizes, and it can exhibit drift under fast irradiance ramps. Contemporary "enhanced IncCond" variants introduce adaptive steps, error-weighted updates, and drift-avoidance logic that significantly reduce settling time and ripple. Such improvements have enabled tracking responses within the sub-tens-of-milliseconds range and overall efficiencies exceeding 99% in both simulation and experimental hardware platforms. In parallel, intelligent alternatives such as fuzzy logic demonstrate high tracking efficiency with complex loads such as batteries, but at the cost of higher design effort and tuning [3].

At the module level, flyback microinverters are appealing due to their galvanic isolation, high step-up capabilities, compact magnetics, and "current source" characteristics that facilitate grid current regulation. Their primary operating modes are discontinuous conduction mode (DCM) and boundary conduction mode (BCM). In BCM and enhanced i-BCM, the transformer completely demagnetizes each cycle, and the switching frequency is significantly influenced by instantaneous power and grid angle, resulting in distinct control interactions for MPPT in contrast to constant-frequency DCM [4].

Research indicates that BCM enhances power density and reduces total harmonic distortion (THD) compared to DCM at similar ratings. However, it also

raises the switching frequency close to grid zero-crossings, which affects efficiency and the timing of sensing and actuation. A hybrid modulation approach that integrates DCM and i-BCM within each half line cycle has been introduced to enhance the high-efficiency envelope and ensure smooth transitions, all while preserving the quality of grid current. The dynamics that depend on the mode suggest that a "mode-aware" MPPT, particularly one that adapts to duty-cycle variations dictated by BCM timing, can enhance the stability of the PV operating point and minimize ripple energy at the MPP [4]-[6].

Several studies examine loss mechanisms in flyback microinverters operating under DCM/BCM, demonstrating the use of phase-shedding or hybrid control to enhance efficiency across varying loads, with MPPT integrated upstream. Most MPPT implementations, however, either assume constant-frequency converters or fail to explicitly consider duty-cycle trajectories that vary predictably with grid angle in BCM [5] [7]. Additionally, the majority of traditional MPPT control strategies are implemented on the voltage-source converter, involving the modification of input voltage and duty cycle. In a current-source system like the flyback-based micro-inverter, direct control of the input voltage is not feasible, as it is contingent upon the characteristics of the photovoltaic (PV) system. The MPPT control approach requires modification and implementation through the adjustment of other variables for application in the PV micro-inverter system [8].

This paper contributes an enhanced incremental conductance MPPT tailored to a flyback-based PV inverter operating in BCM where the duty cycle varies with grid period and input power. The proposed MPPT utilizes a gain scheduling via power zoning approach, adaptively adjusting the input current to the instantaneous BCM duty/frequency to keep a consistent MPP approach rate. Simulation results indicate accurate convergence, lower steady-state ripple, and improved efficiency under different irradiance ramps and PV operating temperature, while preserving the simplicity valued in microinverter applications.

2. Control Strategy

In the BCM flyback-based inverter, especially the single stage type, the peak current control BCM reference current (i_{ref}) is used to control the output current (i_{out}). With the assumption that the input voltage (V_{in}) is constant in the line-frequency cycle, i_{ref} can control the input current (i_{in}) directly. As depicted in **Figure 1**, i_{in} is

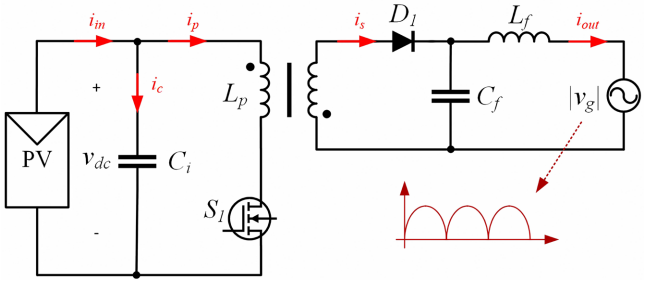

Figure 1. Equivalent circuit of single flyback inverter.

a summation of the capacitor branch current (i_c) and the transformer primary current (i_p). When V_{in} is considered constant in the steady state, i_{in} can be regarded as an average of the transformer's i_p at each switching cycle. The input power (P_{in}) of the inverter can be expressed as (1).

$$P_{in} = \int_0^T v_{dc} i_p \mathrm{d}t \tag{1}$$

2.1. BCM Current Reference (i_{ref}) and MPPT Control Current (I_A)

In this section, the derivation of the BCM reference current and the parameter that interact with the MPPT are elaborated. According to the volt-second balance of the inductance, the turn-on and turn-off time can be deducted as in (2) and (3), while the primary current and secondary current (i_s) relation is realized as in (4) and (5).

$$T_{ON} = L_p \times I_p \times \frac{1}{v_{dc}} \tag{2}$$

$$T_{OFF} = L_s \times I_s \times \frac{1}{v_g} \tag{3}$$

$$I_p = i_{ref} \tag{4}$$

$$I_s = n \times I_p = I_p \sqrt{\frac{L_p}{L_s}} \tag{5}$$

where $\sqrt{L_s / L_p} = n$, the transformer's turn ratio. By considering that the efficiency of the converter is 100%, the amount of power at the output is equal to the input. Therefore, based on **Figure 2**, i_{in} can be calculated according to the assumption that the area of A_1 and A_2 are approximately the equal. i_{in} can be expressed as (6). Likewise, since the i_{out} is yielded from filtering the i_s, the value of the i_{out} is approximately equal to the average value of the secondary current (I_s). Hence, area B_1 and B_2 are considered equal. i_{out} can be expressed as in (7).

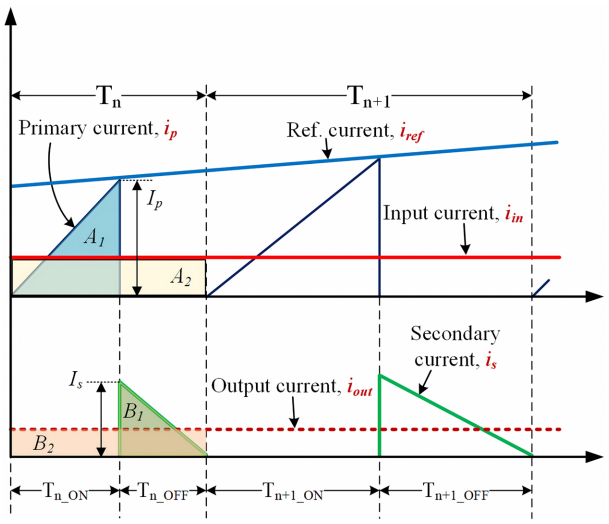

Figure 2. Relation between i_{ref}, i_p, i_s, i_{in}, and i_{out} under BCM.

$$i_{in} = \frac{1}{2} \times I_p \times \frac{T_{ON}}{T_{ON} + T_{OFF}} \tag{6}$$

$$i_{out} = \frac{1}{2} \times I_s \times \frac{T_{OFF}}{T_{ON} + T_{OFF}} \tag{7}$$

Equation (8) is realized to show the relationship between i_{in} and i_{ref} by substituting (2)-(3) into (6). At the steady state condition, the dc voltage v_{dc} and the grid voltage v_g can be considered stable at line-frequency cycle, in which the input current can be controlled directly by the reference current.

$$i_{in} = \frac{1}{2} \times i_{ref} \times \frac{v_g}{v_g + \left(v_{dc} \times \sqrt{L_s / L_p}\right)} \tag{8}$$

Meanwhile, the relationship between i_{ref} and i_{out} in the line-frequency can be expressed in (9) by substituting (2)-(3) into (7). The relationship is deducted by v_g, the transformer's turn ratio and the steady v_{in} due to the selection of large value of input capacitance, C_{in}.

$$i_{ref} = 2i_{out} \times \left(\frac{v_g}{v_{dc}} + \sqrt{\frac{L_s}{L_p}} \right) \tag{9}$$

Subsequently, by solving (8) and (9), the relationship of i_{in} and i_{out} can be expressed as in (10), which proved the instantaneous input power is equivalent to the output power in the ideal condition. According to the standard sinusoidal output current equation, $i_{out} = I_A \sin(\omega t)$, and output voltage $v_g = V_m \sin(\omega t)$, equation (10) can be further expended to (11).

$$i_{in} = i_{out} \times \frac{v_g}{v_{dc}} \tag{10}$$

$$i_{in} = \frac{V_m}{v_{dc}} \times I_A \times \sin^2(\omega t) \tag{11}$$

The expression shows that the i_{in} can be controlled by I_A. This parameter will be interacted and adjusted by MPPT control to track the MPP under BCM operation. I_A is closely related to the output power as shown in (12).

$$I_A = \frac{P_{out}}{V_m} \tag{12}$$

2.2. Enhanced Incremental Conductance

In this work, the flyback-based inverter is a current-source that operates under peak current control and BCM. The duty cycle of the converter will vary throughout line-frequency cycle following the shape of given reference cycle. Therefore, unlike the conventional IncCond that usually alter terminal voltage of the PV panel in accordance with MPP, the proposed modification is altering the terminal current that controlled by the parameter I_A as mentioned in (12). **Figure 3** shows the flowchart of the proposed algorithm. The controller initiates the process by sampling V_{pv} and I_{pv}, subsequently computing P_{pv} and determining the parameter

I_A. In the event that the sequence begins at zero, the initial values for V and I are established at zero, whereas I_{ref} is assigned the calculated value of I_A. Subsequently, the incremental changes in voltage, current, and power are computed at the sampling instant Q.

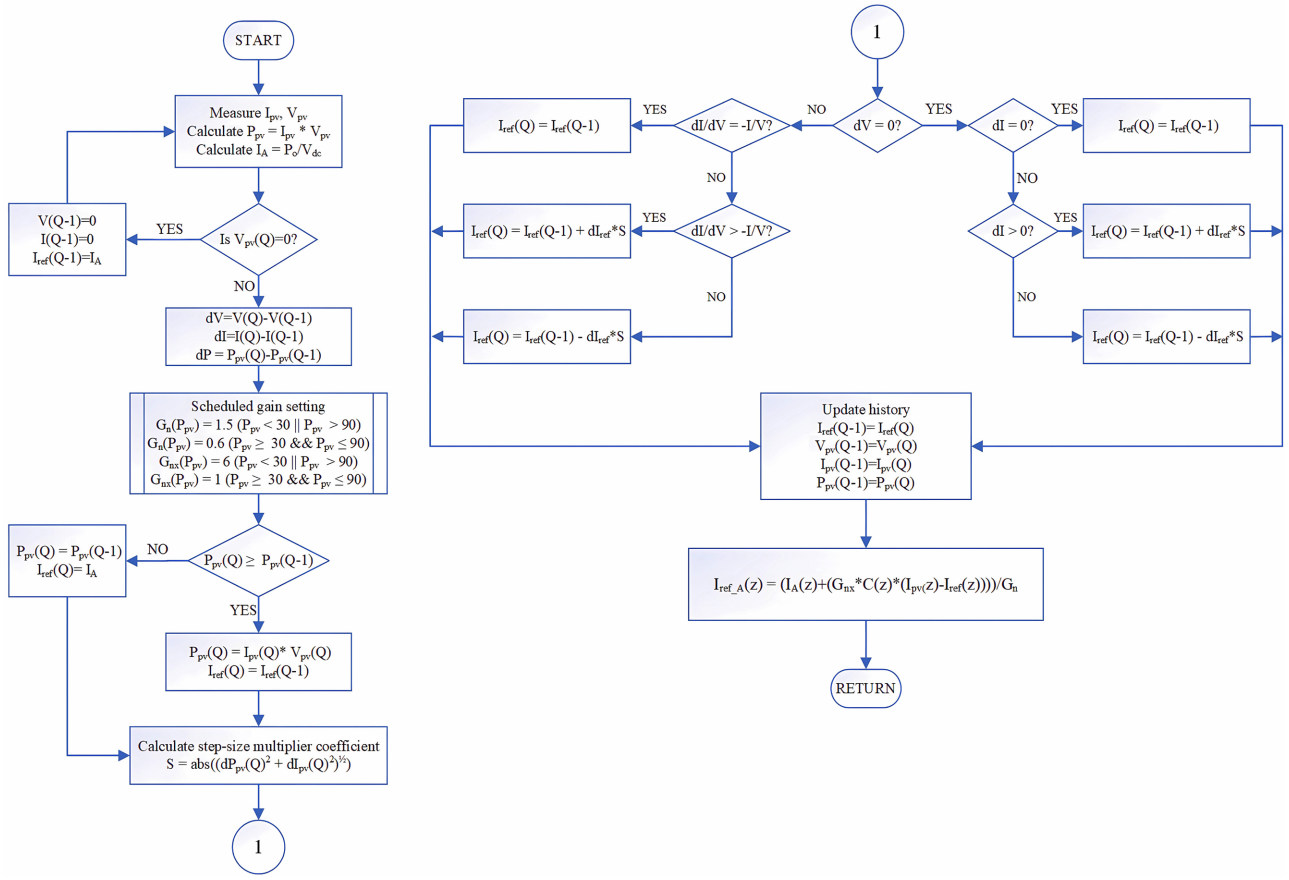

Figure 3. Flowchart of the proposed enhanced InCond MPPT algorithm.

The adjustable reference current is governed by a discrete current law as detailed in (13), with the sign determined by the incremental conductance test. $S[k]$ in Equation (13) represents a step-size multiplier coefficient that scales with the local gradient magnitude, as derived using the Pythagorean theorem in Equation (14). This implements a variable step in incremental conductance, allowing for larger steps when operating point is distant from the MPP to accommodate rapid transients, while minimizing the step size when near to the MPP to mitigate steady-state oscillations. The concept of the Pythagorean theorem was initially applied in P&O by [9] and [10] to address uniform conditions and partial shading conditions, respectively. The adapted I_{ref} is then tracked by an inner current loop as expressed in (15), which includes a PI compensator $C(z)$.

$$I_{ref}[k+1] = I_{ref}[k] \pm dI_{ref} * S[k] \tag{13}$$

$$S = \left|\sqrt{dP^2 + dI^2}\right| \tag{14}$$

$$I_{ref_a} = \frac{I_A(z) + G_{nx}C(z)\left(I_{pv}(z) - I_{ref}(z)\right)}{G_n} \tag{15}$$

To maintain uniform dynamic across the non-linear *I-V* curve, the power zoning with empirical tuning scheduled gains is used, which are applied in (15). The PV operating range is clustered into a mid-power zone (30% - 90% of rated power) and two edge zones (<30% and >90%). The selection of these cluster values is based on the analysis of the MPPT response and characteristics observed across the extensive range of PV power. The nominal loop gain G_n and cross gain G_{nx} are scheduled as explicit functions of the instantaneous PV power P_{pv}, which expressed as a percentage of P_{rated}.

$$G_n\left(P_{pv}\right) = \begin{cases} 1.5, & P_{pv} < 30\% \text{ or } P_{pv} > 90\% \\ 0.6, & 30\% \le P_{pv} \le 90\% \end{cases} \tag{16}$$

$$G_{nx}\left(P_{pv}\right) = \begin{cases} 6.0, & P_{pv} < 30\% \text{ or } P_{pv} > 90\% \\ 1.0, & 30\% \le P_{pv} \le 90\% \end{cases} \tag{17}$$

Aggressive gains in the edge zones enhance recovery when the array functions far from the maximum power point, particularly under conditions of weak irradiance, rapid ramps, or proximity to power clipping, thereby improving transient tracking. In contrast, conservative gains within the 30% - 90% range reduce steady-state ripple and electromagnetic interference (EMI), mitigate current overshoot at rated power, and improve resilience to measurement noise.

3. Simulation Result and Discussion

The proposed IncCond algorithm's functionality and performance have been verified through simulation work conducted with MATLAB/Simulink. **Figure 4** presents the simulation model of the grid-connected interleaved flyback-based inverter, which includes the MPPT block that incorporates the proposed IncCond algorithm. The PV panel used in the simulation is based on the Enedrive DOMETIC's SP-EN100W-24V Mono Solar Panel. Parameters of the simulation

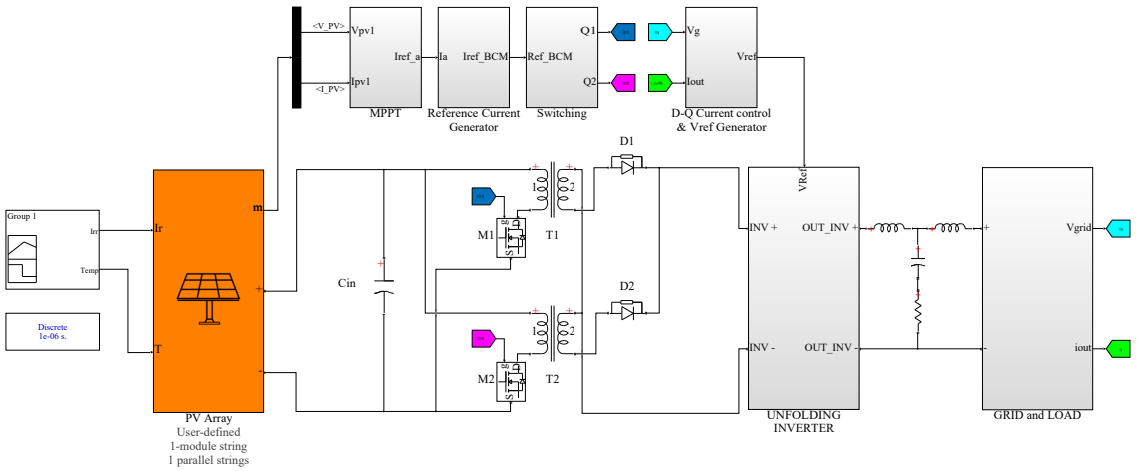

Figure 4. Simulation model of the grid-connected interleaved flyback-based inverter.

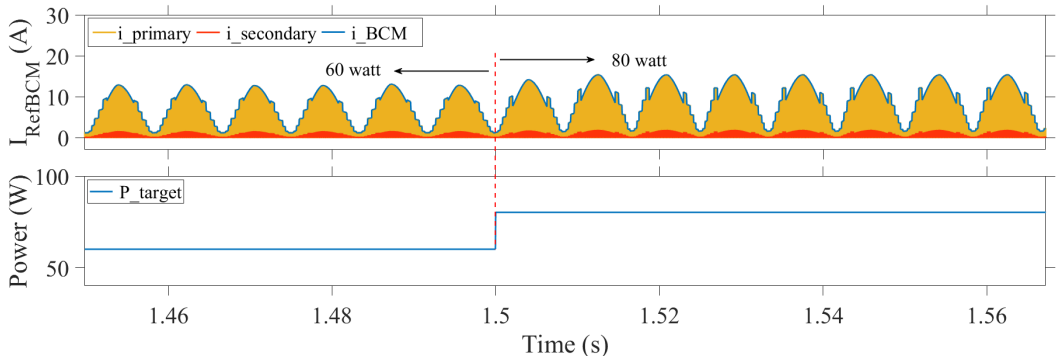

Figure 5. Primary and secondary current response of the inverter under BCM peak current control.

Table 1. Simulation parameters.

Parameter	Symbol	Value	Unit
Transformer magnetizing inductance	L_m	86.6 μ	H
Transformer turn ratio	N	1:7	
Input capacitance	C_{in}	8.8 m	F
Filter capacitance	C_f	1.6 μ	F
Filter inductance	L_1, L_2	6.1 m	H
Filter damping resistor	R_d	10	Ω
Grid voltage	V_g	110	V_{rms}
Solar module max. power	P_{pv_max}	100	W

model are tabulated in Table 1. The current response of the inverter under BCM Peak Current Control is illustrated in Figure 5 during the PV power transition from 60 Watt to 80 Watt. At this point, the inverter is operated under interleaved configuration.

The proposed algorithm was validated through the application of a uniform solar irradiance step size of 200 W/m^2, 300 W/m^2, 600 W/m^2, 800 W/m^2, and 1000 W/m^2. Each level of irradiance was sustained for a duration of 0.5 seconds. The results are consolidated in Figure 6. The upper plot illustrates the performance of PV power tracking, whereas the lower plot represents the associated reference current response. The upper plot illustrates that the PV power aligns closely with the targeted reference at each irradiance step. This demonstrates the effectiveness of the proposed MPPT in achieving rapid and precise tracking under various operating conditions. The transitions between irradiance levels exhibit a smooth convergence with minimal steady-state error. The bottom plot illustrates the dynamics of the reference current, which display clear oscillatory patterns as the algorithm continuously adjusts to ensure alignment between the actual and targeted power levels. At lower irradiance levels, the oscillations are minimal and rapidly attenuated. In contrast, at elevated power levels, more significant oscillations emerge due to the increased energy exchanges necessary for the adjustment process. The oscillations are notably well bounded and do not lead to system destabi-

lization, demonstrating the algorithm's capability to maintain a balance between rapid transient adaptation and stable long-term performance.

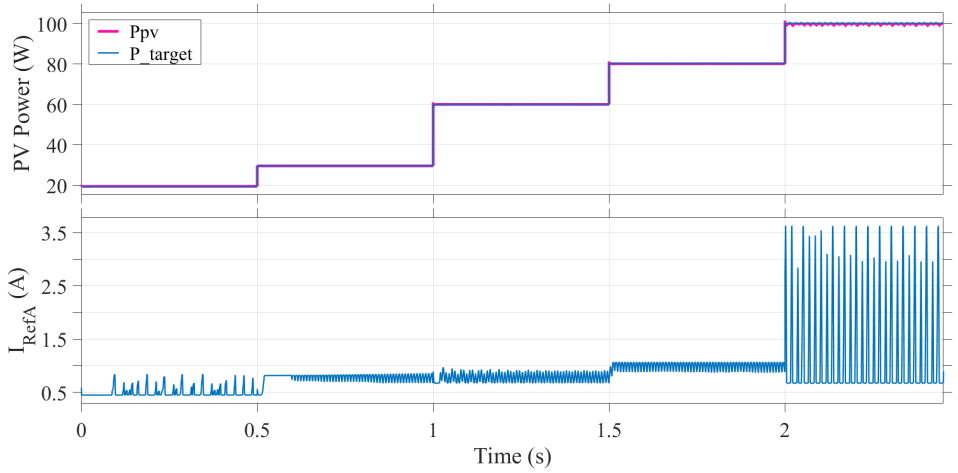

Figure 6. PV power and MPPT reference current response under different irradiance level.

The efficacy of the proposed MPPT in regulating PV power toward the targeted value is illustrated in **Figure 7**. The upper plot shows that the actual PV power nearly aligns with the desired power, exhibiting only minor deviation near the setpoint. These small discrepancies are promptly corrected, reflecting the high precision and responsiveness of the control algorithm. The lower plot elucidates the correction mechanism, demonstrating that the reference current displays discrete step-like variations in response to power mismatches. Each increment or decrement in current reflects an adaptive adjustment initiated by the controller to realign the PV power with the reference value. This mechanism ensures rapid convergence while avoiding instability or excessive oscillations.

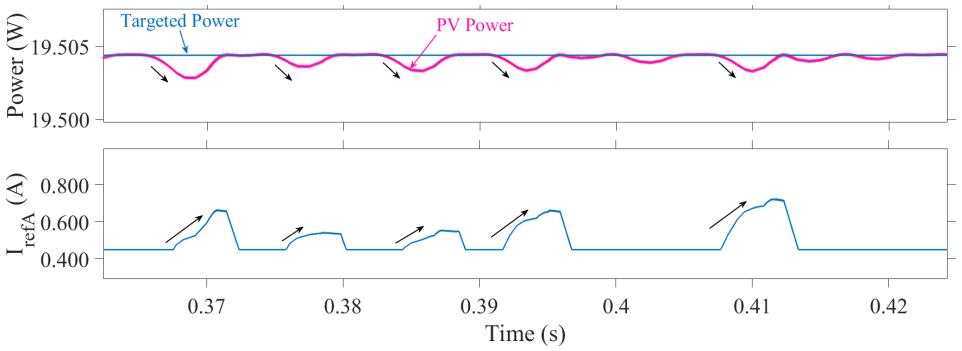

Figure 7. MPPT reference current retification mechanism to stabileze MPP.

Figure 8 demonstrates the dynamic performance of the proposed MPPT in response to a step change in the desired power reference. For instance, as the target rises from 60 Watt to 80 Watt, the PV output power reacts almost instantaneously, closely aligning with the new setpoint and exhibiting only a slight transient deviation. The magnified perspective of the transition edge reveals a short overshoot,

during which the power momentarily surpasses the reference before rapidly stabilizing within a narrow steady-state error range of less than ±1 Watt. This behavior indicates a rapid but well-controlled transient response, showcasing the algorithm's capability for swift tracking while maintaining stability. The lower inset elucidates the control mechanism where the reference current demonstrates bounded oscillations as the controller compensates for overshoot and ensures alignment with the new power target.

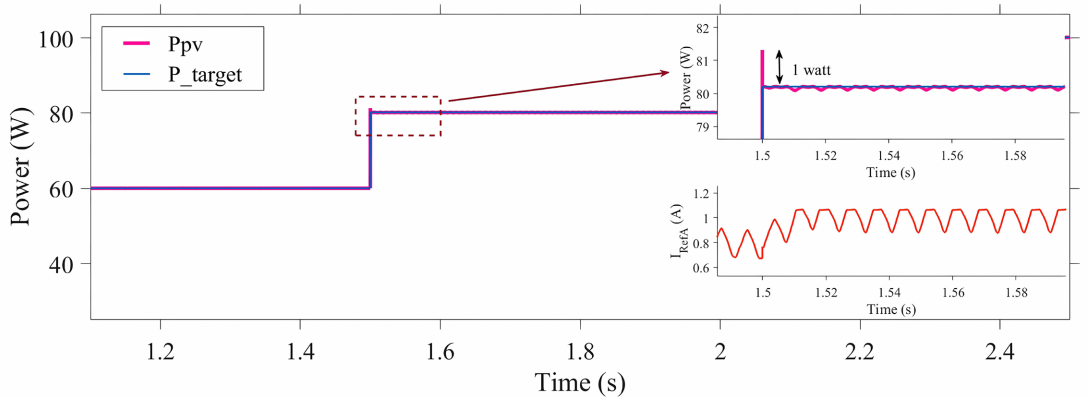

Figure 8. Dynamic performance of the proposed MPPT in respond to step chance.

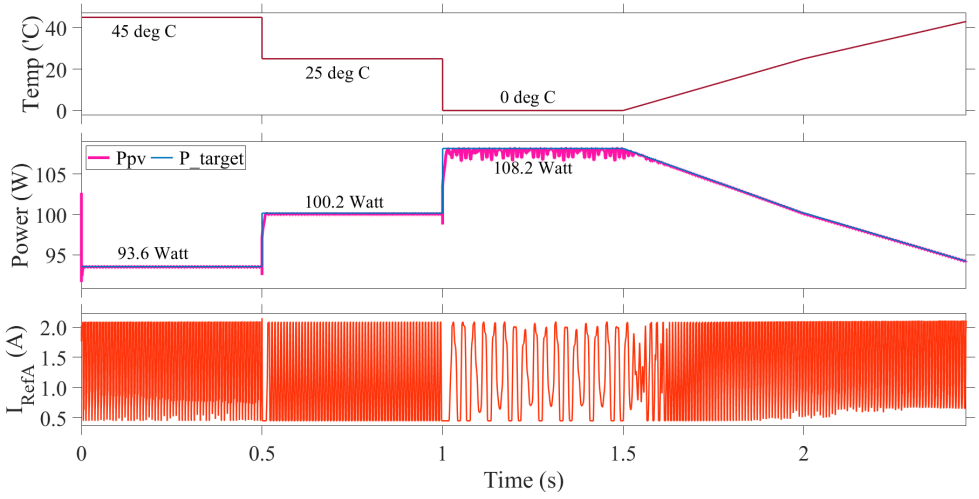

Figure 9. PV power response across different temperature conditions.

The proposed algorithm is further validated with a varying PV panel temperature. In the previous simulation the test was conducted at a uniform room temperature, *i.e.*, 25˚C at different irradiance levels. With varying temperature configuration, the test is set at uniform 1000 W/m^2 irradiance. **Figure 9** illustrates the PV power response across different temperature conditions, highlighting both transient and steady-state response of the PV system. The upper plot illustrates the applied temperature profile, exhibiting a decremental pattern in distinct intervals from 45˚C to 25˚C, subsequently to 0˚C, followed by a gradual increase. As expected, these temperature variations directly influence the PV power output,

as depicted in the middle plot. As the temperature decreases, there is an increase in PV power attributed to enhanced voltage-current characteristics of the solar module. The proposed controller effectively tracks the new maximum power point at each condition. The PV power output transitions from approximately 93.6 Watt at 45˚C to 100.2 Watt at 25˚C, and further increases to 108.2 Watt at 0˚C. These values closely align with the targeted reference, exhibiting negligible steady-state errors. Even during the continuous rise in temperature beyond 0˚C, the PV power smoothly follows the decreasing target, showcasing the MPPT's strong adaptability to non-step changes. The bottom plot provides additional insight into control behavior, where the reference current exhibits oscillatory patterns reflecting the algorithm's active adjustment to power variations caused by temperature changes.

Further analysis on the step response shows some effect during the temperature change at 1000 W/m^2. **Figure 10** shows the transient and steady state response and the magnified view during the temperature change from 25˚C to the extreme 0˚C. As observed, when the reference increased from 100 Watt to 108 Watt, the actual power rapidly follows the new set point with minimal negative overshoot of about 1.4 Watt. Whereas the magnified inset highlights the transient behavior, where the PV power settles within 16 milliseconds. Importantly, the steady-state tracking error remains negligible, with the PV output consistently aligned with reference despite small fluctuations. The lower plot further explains the correction mechanism through the reference current, which exhibits bounded oscillations during the transition phase.

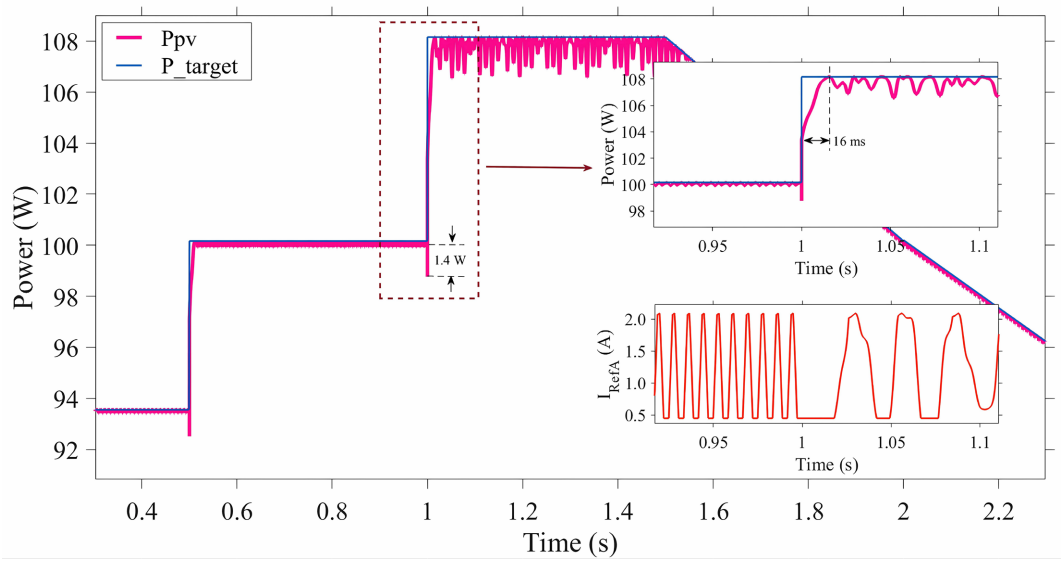

Figure 10. The transient and steady state response during the temperature change.

4. Conclusion

In this paper, an enhanced version of Incremental Conductance approach to track the maximum power point for a flyback-based inverter was proposed and vali-

dated. A Matlab/Simulnik based simulation of a grid connected PV system was conducted to verify and validate the proposed approach under uniform temperature with varies irradiance and with variable temperature under uniform solar irradiance. The result from the simulation shows that the proposed algorithm tracks the MPP with negligible overshoot during irradiance or temperature abrupt change. It has been also observed that the oscillation is minimum within the operational region and system rated power. A slightly rough oscillation is observed when the PV is operated at extreme operating temperature conditions *i.e.*, 0˚C. However, the algorithm able to rectify the deviation with less than 2 Watt overshoot and within 16 milliseconds settling time.

Acknowledgements

The authors would like to thank Universiti Teknikal Malaysia Melaka and Universiti Putra Malaysia for their financial and technical support.

Conflicts of Interest

The authors declare no conflicts of interest regarding the publication of this paper.

References

[1] Chellakhi, A., El Beid, S., Abouelmahjoub, Y. and Doubabi, H. (2024) An Enhanced Incremental Conductance MPPT Approach for PV Power Optimization: A Simulation and Experimental Study. *Arabian Journal for Science and Engineering*, **49**, 16045-16064. https://doi.org/10.1007/s13369-024-08804-1

[2] Asoh, D.A., Noumsi, B.D. and Mbinkar, E.N. (2022) Maximum Power Point Tracking Using the Incremental Conductance Algorithm for PV Systems Operating in Rapidly Changing Environmental Conditions. *Smart Grid and Renewable Energy*, **13**, 89-108. https://doi.org/10.4236/sgre.2022.135006

[3] Baramadeh, M.Y., Abouelela, M.A.A. and Alghuwainem, S.M. (2021) Maximum Power Point Tracker Controller Using Fuzzy Logic Control with Battery Load for Photovoltaics Systems. *Smart Grid and Renewable Energy*, **12**, 163-181. https://doi.org/10.4236/sgre.2021.1210010

[4] Christidis, G.C., Nanakos, A.C. and Tatakis, E.C. (2016) Hybrid Discontinuous/Boundary Conduction Mode of Flyback Microinverter for AC-PV Modules. *IEEE Transactions on Power Electronics*, **31**, 4195-4205. https://doi.org/10.1109/tpel.2015.2470094

[5] Yaqoob, S.J., Raham, J.K. and Sadiq, H.A. (2021) Analysis and Simulation of Current-Source Flyback Inverter with Efficient BCM Control Strategy. *WSEAS Transactions on Electronics*, **12**, 132-140. https://doi.org/10.37394/232017.2021.12.18

[6] Yaakub, M.F., *et al.* (2021) BCM-CPC Flyback Micro-Inverter for Grid-Connected Photo-Voltaic Application. *Proceesings of Malaysian Technical Universities Conference on Engineering and Technology* (*MUCET*) 2021, Melaka, 16-18 November 2021, 55-56.

[7] Zhang, Y., He, X., Zhang, Z. and Liu, Y. (2013) A Hybrid Control Method for Photovoltaic Grid-Connected Interleaved Flyback Micro-Inverter to Achieve High Efficiency in Wide Load Range. 2013 *Twenty-Eighth Annual IEEE Applied Power Electronics Conference and Exposition* (*APEC*), Long Beach, 17-21 March 2013, 751-756.

https://doi.org/10.1109/apec.2013.6520294

[8] Ansari, S.A., Skandari, A., Milimonfared, J. and Moghani, J.S. (2018) A New Control Method for an Interleaved Flyback Inverter to Achieve High Efficiency and Low Output Current THD. 2018 9*th Annual Power Electronics*, *Drives Systems and Technologies Conference* (*PEDSTC*), Tehran, 13-15 February 2018, 89-94. https://doi.org/10.1109/pedstc.2018.8343777

[9] Loukriz, A., Messalti, S. and Harrag, A. (2019) Design, Simulation, and Hardware Implementation of Novel Optimum Operating Point Tracker of PV System Using Adaptive Step Size. *The International Journal of Advanced Manufacturing Technology*, **101**, 1671-1680. https://doi.org/10.1007/s00170-018-2977-7

[10] Mahmod Mohammad, A.N., Mohd Radzi, M.A., Azis, N., Shafie, S. and Atiqi Mohd Zainuri, M.A. (2020) An Enhanced Adaptive Perturb and Observe Technique for Efficient Maximum Power Point Tracking under Partial Shading Conditions. *Applied Sciences*, **10**, Article 3912. https://doi.org/10.3390/app10113912